PHYSICAL REVIEW A **78**, 063801 (2008)

# Demonstration of a bright and compact source of tripartite nonclassical light

Alessia Allevi
*UdR Como, CNISM, I-22100, Como, Italy*

Maria Bondani*
*National Laboratory for Ultrafast and Ultraintense Optical Science, CNR-INFM and UdR Como, CNISM, I-22100, Como, Italy*

Matteo G. A. Paris
*Dipartimento di Fisica, Università degli Studi di Milano, Milano, Italy;*
*UdR Milano, CNISM, I-20133 Milano, Italy;*
*and ISI Foundation, I-10133 Torino, Italy*

Alessandra Andreoni
*Dipartimento di Fisica e Matematica, Università degli Studi dell'Insubria, Como, Italy*
*and UdR Como, CNISM, I-22100, Como, Italy*
(Received 16 May 2008; published 1 December 2008)

We experimentally demonstrate the nonclassical photon number correlations expected in tripartite continuous-variable states obtained by parametric processes. Our scheme involves a single nonlinear crystal, where two interlinked parametric interactions take place simultaneously, and represents a bright and compact source of a sub-shot-noise tripartite light field. We analyze the effects of the pump intensities on the numbers of detected photons and on the amount of noise reduction in some detail, thus demonstrating a good agreement between the experimental data and a single-mode theoretical description.

DOI: 10.1103/PhysRevA.78.063801 PACS number(s): 42.50.Ar, 42.50.Dv, 42.65.Lm

## I. INTRODUCTION

Multimode light beams endowed with nonclassical correlations, as those exhibited by multipartite entangled states, represent a resource for quantum technology. They are at the heart of enhanced quantum imaging, either ghost imaging or ghost diffraction [1,2], and represent a building block for the development of an integrated quantum network. In turn, nonlinear interactions involving multimode beams of radiation have attracted much attention in the recent years, either to realize all-optical information processing [3] or to generate nonclassical states of light [4]. Several experimental schemes to generate multimode entangled states have been suggested and demonstrated. The first example is provided by the original continuous-variable (CV) teleportation experiments in Ref. [5], where one mode of a twin beam was mixed with a coherent state, although no specific analysis was made of the entanglement properties besides the verification of teleportation. A similar scheme, where one mode of a twin beam is mixed with the vacuum, has been demonstrated and applied to controlled dense coding [6]. Moreover, a fully inseparable three-mode entangled state has been generated and verified by mixing three independent squeezed vacuum states in a network of beam splitters [7]. Recently we suggested and demonstrated a compact scheme to realize three-mode entanglement by means of two interlinked $\chi^{(2)}$ interactions occurring in a single nonlinear crystal in a type-I noncollinear phase-matching geometry [8,9]. Other schemes involving cascaded interactions have also been analyzed either in periodically poled crystals [10] or in second-order nonlinear ones [11–13]. Notice, however, that the use of a single nonlinear medium makes the system more compact and robust compared to the other schemes that have been suggested and demonstrated so far, in which additional parametric sources and linear devices, such as beam splitters, introduce unavoidable losses. Finally, parametric oscillators have been suggested as a source of tripartite signal-idler-pump entanglement in triply resonant cavities [14].

In this paper we experimentally demonstrate the nonclassical photon correlations exhibited by tripartite states generated by a single nonlinear crystal, where two interlinked parametric interactions take place simultaneously. Our scheme realizes a bright and compact source of sub-shot-noise three-mode light beams and allows the implementation of simultaneous ghost imaging and ghost diffraction protocols with enhanced sensitivity.

The paper is structured as follows. In the next section we provide a theoretical description of our system and evaluate correlations and noise reduction as a function of the coupling parameters. In Sec. III we describe our experimental apparatus, illustrate the results with focus on nonclassical photon-number correlations, and analyze the sources of noise in some details. Section IV closes the paper with some remarks.

## II. THEORETICAL DESCRIPTION

In our scheme two interlinked interactions, namely, a spontaneous parametric down-conversion process and a sum-frequency generation, take place simultaneously in a single nonlinear crystal. In principle, five modes $a_j$ are involved in the interactions, two of which, say $a_4$ and $a_5$, are nonevolv-

*maria.bondani@uninsubria.it

 ©2008 The American Physical Society

ing undepleted pumps and thus are included in the coupling coefficients (parametric approximation). The effective Hamiltonian describing the interaction is thus given by

$$H_{\rm int} = g_1 a_1^\dagger a_3^\dagger + g_2 a_2^\dagger a_3 + \text{H.c.}, \tag{1}$$

where $g_1$ and $g_2$ are coupling coefficients linearly dependent on the pump fields $a_4$ and $a_5$, respectively. The earliest studies on the dynamics and the quantum properties of the states realized via this Hamiltonian can be traced back to the works in Refs. [15,16]. The relevance of studying the dynamics generated by the above Hamiltonian in details lies in the fact that $H_{\rm int}$ can be realized in a variety of different contexts, from quantum optics [10,12,17–19] to condensate physics [20,21]. The coupling between two optical modes and one vibrational mode of a macroscopic object, such as a mirror, has been considered [22], and also ions trapped in a cavity have been demonstrated to realize the Hamiltonian in Eq. (1) for a suitable configuration [23].

The Hamiltonian admits the constant of motion $\Delta(t) \equiv N_1(t) - N_2(t) - N_3(t) \equiv \Delta(0)$. If we take the vacuum $|\mathbf{0}\rangle \equiv |0\rangle_1 \otimes |0\rangle_2 \otimes |0\rangle_3$ as the initial state, we have $N_1(t) = N_2(t) + N_3(t) \,\forall\, t$, where $N_j(t) = \langle a_j^\dagger(t) a_j(t)\rangle$ is the mean number of photons in the $j$th mode. Under these hypotheses the evolved state $|\mathbf{T}\rangle = \exp\{-iH_{\rm int}t\}|\mathbf{0}\rangle$ may be written as

$$|\mathbf{T}\rangle = \sum_{mr} \frac{N_2^{m/2} N_3^{r/2}}{(1+N_1)^{(1+m+r)/2}} \sqrt{\frac{(m+r)!}{m!r!}} |m+r, m, r\rangle, \tag{2}$$

where we omitted the time dependence of $N_j$. As a matter of fact, the state in Eq. (2) is a fully inseparable three-mode Gaussian state [24], i.e., a state that is inseparable with respect to any grouping of the modes, thus permitting realizations of truly tripartite quantum protocols such as conditional twin-beam generation and telecloning [17,18]. The mean numbers of photons $N_j$ that appear in Eq. (2) can be obtained by the Heisenberg evolution of the field operators. In particular, by introducing $\Omega = \sqrt{|g_2|^2 - |g_1|^2}$ we have $N_1 = N_2 + N_3$ and

$$N_2 = \frac{|g_1|^2 |g_2|^2}{\Omega^4} (\cos \Omega t - 1)^2, \quad N_3 = \frac{|g_1|^2}{\Omega^2} \sin^2(\Omega t). \tag{3}$$

We see that when $|g_2|^2 > |g_1|^2$ the dynamics is oscillatory; vice versa, when $|g_1|^2 > |g_2|^2$ we find an exponential behavior.

The above description of the system has been derived under the hypothesis of perfect frequency-matching and phase-matching conditions among single-mode fields, and the time $t$ appearing in Eqs. (3) represents the interaction time inside the crystal. In this case we did not need to take into account the existence of temporal modes and spatial coherence areas. On the other hand, if the pump fields are pulsed, the generated fields are temporally multimode [25]. Moreover, in a noncollinear interaction geometry, the momentum conservation in the transverse direction can be satisfied in more than one way. Thus coherence areas exist [24,26], whose angles of divergence depend on several parameters, such as the pumps intensities, the distance from the collinear interaction geometry and the wavelengths of the generated fields. It is interesting to point out that in the CV regime the demonstration of the entangled nature of the state in Eq. (2) critically depends on the correct collection of these coherence areas [27]. In fact, collecting light from more than a single coherence area corresponds to the introduction of spurious light, while collecting less than a coherence area determines a loss of information, which is detrimental to the investigations of the nonclassical properties. In addition, we have to select a triplet of areas as there is a one-to-one correspondence between the coherence areas in each field. To achieve such a selection we can apply a criterion which represents a necessary but not sufficient condition, based on the study of the correlation in the number of photons. In fact, due to the constant of motion, the state in Eq. (2) is endowed with perfect correlations in the number of photons. The three-mode photon-number distribution is given by

$$P_T(n,m,r) = \delta_{n,m+r} \frac{N_2^m N_3^r}{(1+N_1)^{1+m+r}} \frac{(m+r)!}{m!r!}, \tag{4}$$

from which we can derive the photon-number correlation coefficients between the components of the entangled state. In particular, due to the conservation law, we expect the existence of strong intensity correlations between the number of photon $n_1$ and the sum of the other two, say $n_2 + n_3$. In order to quantify correlations we denote by $\gamma(n_j, n_k) = \langle n_j n_k\rangle - \langle n_j\rangle\langle n_k\rangle$ and $\sigma^2(n_j) = \langle n_j^2\rangle - \langle n_j\rangle^2$ the covariance and the variance of the number of photons, respectively, and introduce the correlation coefficients as follows:

$$\epsilon_{j,k} = \frac{\gamma(n_j, n_k)}{\sigma(n_j)\sigma(n_k)}. \tag{5}$$

Upon exploiting Eq. (4) we have that the correlation coefficient $\epsilon_{1,2+3}$ is identically equal to 1, independently of the number of photons generated by the interlinked interactions. On the other hand, for the partial photon-number correlations we obtain expressions that do depend on the mean number of photons involved. Upon writing $N_k = \beta_k N$ where $\beta_1 = \beta_2 + \beta_3$ and $N$ is the total number of photons of the state, we have

$$\epsilon_{1,k} = \sqrt{\frac{N_k(1+N_1)}{N_1(1+N_k)}} \overset{N\gg 1}{\simeq} 1 - \frac{\beta_1 - \beta_k}{2\beta_1\beta_k N}, \tag{6}$$

$$\epsilon_{2,3} = \sqrt{\frac{N_2 N_3}{(1+N_2)(1+N_3)}} \overset{N\gg 1}{\simeq} 1 - \frac{\beta_2 + \beta_3}{2\beta_2\beta_3 N}, \tag{7}$$

where from now on $k = 2,3$. As the detectors we used to perform the correlation measurements are not ideal, we have to rewrite the expressions of the correlation coefficients by taking into account the nonunit quantum efficiency of the detection apparatus. The probability operator-valued measure of each detector, describing the statistics of detected photons, is given by a Bernoullian convolution of the ideal number operator spectral measure

$$\hat{\Pi}_{m_j} = \eta_j^{m_j} \sum_{n_j = m_j}^{\infty} (1-\eta_j)^{n_j - m_j} \binom{n_j}{m_j} |n_j\rangle\langle n_j| \tag{8}$$

with $j = 1,2,3$. Equation (8) can be exploited to calculate the expressions of mean number $\langle m_j\rangle$ and variance $\sigma^2(m_j)$ of the detected photons $m_j$ in terms of the mean number of photons $n_j$ and its variance $\sigma^2(n_j)$ [31],

$$M_j \equiv \langle m_j \rangle = \eta_j \langle n_j \rangle = \eta_j N_j,$$

$$\sigma^2(m_j) = \eta_j^2 \sigma^2(n_j) + \eta_j(1-\eta_j)N_j. \tag{9}$$

We notice that, in general, the statistical distribution of the number of detected photons is different from that of the number of photons. Nevertheless, the correlation coefficients $\epsilon^m$ calculated for the detected photons can also assume high values; in particular, the correlation coefficient calculated between $m_1$ and the sum $m_2+m_3$ reads as follows:

$$\epsilon^m_{1,2+3} = \frac{\eta(1+N_1)}{(1+\eta N_1)} \overset{N\gg 1}{\simeq} 1 - \frac{1-\eta}{\eta}\frac{1}{\beta_1 N}, \tag{10}$$

where we have assumed that all the detectors have the same quantum efficiency $\eta$. In turn, the partial correlations are given by

$$\epsilon^m_{1,k} \overset{N\gg 1}{\simeq} 1 - \frac{\beta_1+\beta_k-2\eta\beta_k}{2\beta_1\beta_k N}, \tag{11}$$

$$\epsilon^m_{2,3} \overset{N\gg 1}{\simeq} 1 - \frac{\beta_2+\beta_3}{2\eta\beta_2\beta_3 N}, \tag{12}$$

and approach unit value for large $N$ values.

As a matter of fact a large value of the correlation indices is not sufficient to discriminate between quantum and classical correlations [31]. A trivial example is given by the mixture $\varrho = \Sigma_{nmr} P_T(n,m,r)|n\rangle\langle n| \otimes |m\rangle\langle m| \otimes |r\rangle\langle r|$, which, with $P_T(n,m,r)$ given as in Eq. (4), exhibits the same correlations as the state $|\mathbf{T}\rangle$. A more realistic example is provided by the tripartite state generated by sending a thermal state on two subsequent beam splitters, whose second port is unexcited: the state is classical and shows large intensity correlations, approaching unit value for large mean photon numbers [28].

In order to obtain a proper marker of nonclassicality we may take into account the difference photocurrents $d_{j,k}=m_j - m_k$ [27] and build the so-called noise reduction factor

$$R_{j,k} = \frac{\sigma^2(d_{j,k})}{\langle m_j \rangle + \langle m_k \rangle}, \tag{13}$$

which is smaller than 1 for nonclassically correlated states. Note also that, for states generated by the Hamiltonian in Eq. (1), the existence of sub-shot-noise photon-number correlations is a sufficient condition for entanglement, i.e., the condition of negative partial transpose is subsumed by the condition of sub-shot-noise correlations [18]. By using Eqs. (9) we may write

$$R_{j,k} = 1 - \eta + \frac{\eta[\sigma^2(n_j)+\sigma^2(n_k)-2\gamma(n_j,n_k)]}{\langle n_j \rangle + \langle n_k \rangle} \tag{14}$$

for the noise reduction of bipartite correlations whereas, for the difference photocurrent between the mode $a_1$ and the sum of the other two modes, we have $R \equiv R_{1,2+3}$,

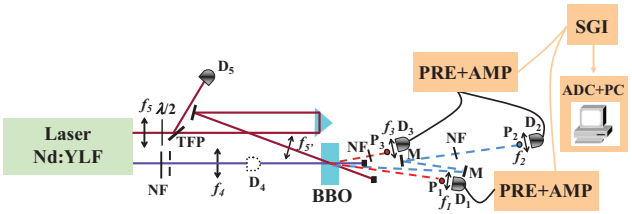


FIG. 1. (Color online) Scheme of the experimental setup: BBO, nonlinear crystal; NF, variable neutral-density filter; $\lambda/2$, half-wave plate; TFP, thin-film plate polarizer; $P_1$–$P_3$, pinholes; $f_1$–$f_{5'}$, lenses; $D_1$–$D_3$, *p-i-n* photodiodes; $D_4$, $D_5$, thermal detectors; $M$, aluminum mirrors; PRE+AMP, low-noise charge-sensitive preamplifiers followed by amplifiers; SGI, synchronous gated integrator; ADC+PC, computer-integrated digitizer.

$$R = 1 - \eta + \frac{\eta\left(\sum_p \sigma^2(n_p) + 2\Gamma(\{n_k\})\right)}{\sum_p \langle n_p \rangle}, \tag{15}$$

where

$$\Gamma(\{n_k\}) = \gamma(n_2,n_3) - \gamma(n_1,n_2) - \gamma(n_1,n_3). \tag{16}$$

For the state in Eq. (2) we have

$$R = 1 - \eta, \tag{17}$$

which shows that state $|\mathbf{T}\rangle$ exhibits nonclassical tripartite correlations for any value of the mean number of photons. In addition, Eq. (17) says that the noise reduction can be detected for any value of the quantum efficiency $\eta$. The corresponding bipartite quantities read as follows:

$$R_{1,k} = 1 + \frac{\eta[(N_1-N_k)^2 - 2N_k]}{N_1+N_k} \overset{N\gg 1}{\simeq} \eta N \frac{(\beta_1-\beta_k)^2}{\beta_1+\beta_k}, \tag{18}$$

$$R_{2,3} = 1 + \frac{\eta(N_2-N_3)^2}{N_2+N_3} \overset{N\gg 1}{\simeq} \eta N \frac{(\beta_2-\beta_3)^2}{\beta_2+\beta_3}, \tag{19}$$

and say that the correlations between modes $a_2$ and $a_3$ are always classical, whereas the correlations between mode $a_1$ and either mode $a_2$ or mode $a_3$ may be nonclassical in certain regimes. More specifically, we have $R_{1,k}<1$ if $N_1<N_k+\sqrt{2N_k}$. Since $N_1=N_2+N_3$ we may have both the noise reduction parameters below the classical threshold only for an overall energy of the state $N_1+N_2+N_3<4$.

## III. EXPERIMENT

The experimental scheme used to generate the nonclassical state of Eq. (2) is depicted in Fig. 1. The harmonics of a continuous-wave mode-locked Nd:YLF (yttrium lithium fluoride) laser regeneratively amplified at a repetition rate of 500 Hz (High Q Laser Production, Hohenems, Austria) provide the two pump fields. In particular, the third harmonic pulse at 349 nm (~4.45 ps pulse duration) is exploited as the pump field $a_4$ in the down-conversion process, whereas the fundamental pulse at 1047 nm (~7.7 ps pulse duration) is used as the pump field $a_5$ in the up-conversion process. The

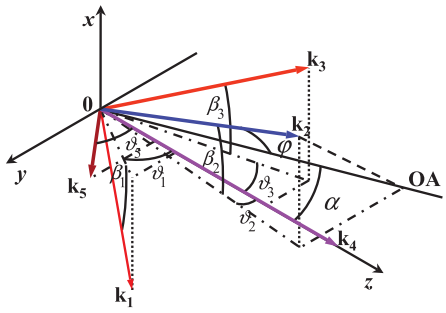


FIG. 2. (Color online) Scheme of the phase-matched interlinked interactions: $(x,y)$ plane coincides with the crystal entrance face; $\alpha$, tuning angle; $\beta_j$'s, angles to $(y,z)$ plane; $\vartheta_j$'s, angles on the $(y,z)$ plane; $\varphi$, angle to the optical axis (OA).

two processes must simultaneously satisfy energy-matching ($\omega_4=\omega_1+\omega_3$, $\omega_2=\omega_3+\omega_5$) and phase-matching ($\mathbf{k}_4^e=\mathbf{k}_1^o+\mathbf{k}_3^o$, $\mathbf{k}_2^e=\mathbf{k}_3^o+\mathbf{k}_5^o$) conditions, in which $\omega_j$ are the angular frequencies, $\mathbf{k}_j$ are the wave vectors and superscripts $o,e$ indicate ordinary and extraordinary field polarizations. As depicted in Fig. 2, we set the pump-field $a_4$ direction so that the wave vector $\mathbf{k}_4$ is normal to the crystal entrance face and propagates along the $z$ axis of the medium. We also align the wave vector $\mathbf{k}_5$ of the other pump field $a_5$ in the plane $(y,z)$ containing the optical axis of the crystal and the wave vector $\mathbf{k}_4$. The nonlinear medium is a $\beta$-$BaB_2O_4$ crystal (BBO, Fujian Castech Crystals, China, $10\times10$ mm$^2$ cross section, 4 mm thickness) cut for type-I interaction ($\vartheta_{\text{cut}}=38.4°$), into which both pumps are strongly focused. Typical intensity values of the pumps were $\sim5$ GW/cm$^2$ for $a_4$ and $\sim2$ GW/cm$^2$ for $a_5$. The required superposition in time of the two pumps is obtained by a variable delay line.

With reference to Fig. 2, we indicate as $\vartheta_j$ the angles in the plane $(y,z)$ formed by each wave vector with $\mathbf{k}_4$ and as $\beta_j$ the angles of each wave vector with respect to this plane. For the experimental realization of the interaction scheme we choose the solutions in the plane $(y,z)$, thus $\beta_j=0$ for $j=1-3$: in particular, we sent the pump field $a_5$ at an external angle $\vartheta_{5,\text{ext}}=-24.47°$ with respect to the other pump field $a_4$. Under these hypotheses, for $\lambda_1=632.8$ nm, $\lambda_2=446.4$ nm, and $\lambda_3=778.2$ nm, we calculated the following external interaction angles with respect to the pump field $a_4$: $\vartheta_{1,\text{ext}}=-9.78°$, $\vartheta_{2,\text{ext}}=-3.25°$, and $\vartheta_{3,\text{ext}}=+12.06°$ [9].

The preliminary use of a He:Ne laser as the seed field allowed us to position three pinholes on the path of the three generated fields in such a way that then, when operating the system from vacuum (i.e., in the absence of any seed fields), we could collect a triplet of coherence areas. Distances and sizes of the pinholes were chosen by searching for the condition of maximum intensity correlations between the generated fields [28]. In fact, as shown in Sec. II, we expect strong intensity correlations not only between the number of detected photons $m_1$ and the sum of the other two, but also between $m_1$ and $m_2$, $m_2$ and $m_3$, and $m_1$ and $m_3$. By applying this criterion, we finally decided to put two pinholes of 30 $\mu$m diameter at distances $d_1=60$ cm and $d_3=49$ cm from the BBO along the path of the signal beam at 632.8 nm and of the idler beam at 778.2 nm, respectively. The two different distances were chosen to compensate for the difference in the divergence of signal and idler due to their wavelengths [24]. Moreover, as the beam at 446.4 nm has a divergence smaller than those of the other two fields, we selected it by means of a 50 $\mu$m diameter pinhole placed at a distance $d_2=141.5$ cm from the crystal.

The light, suitably filtered by means of bandpass filters located in front of each pinhole, was focused on each detector by a lens ($f_1=f_3=25$ mm, $f_2=10$ mm). Since we performed measurements in the macroscopic intensity regime (more than 1000 photons per coherence area), we used three *p-i-n* photodiodes (two, $D_{1,2}$ in Fig. 1, S5973-02 and one, $D_3$, S3883, Hamamatsu, Japan) as the detectors. In order to obtain the same overall detection efficiency (bandpass filter plus detector) on the three arms, we put two adjustable neutral-density filters in the pathways of $a_2$ and $a_3$, thus obtaining the same value $\eta=0.28$ on the three arms. The current output of the detectors was amplified by means of two low-noise charge-sensitive preamplifiers (CR-110, Cremat, Watertown, MA) followed by two amplifiers (CR-200-4 $\mu$s, Cremat). We connected the detectors $D_2$ and $D_3$ to the same amplifier device by means of a T adapter. The two amplified outputs were then integrated by synchronous gated integrators (SGI in Fig. 1) operating in external trigger modality (SR250, Stanford Research Systems, Palo Alto, CA). The voltage outputs were then sampled, digitized by a 12-bit converter (AT-MIO-16E-1, DAQ National Instruments) and recorded by a computer.

In the following we discuss the measurements of the intensities of field $a_1$ and of the sum $a_2+a_3$ as, according to Eqs. (17)–(19), we expect a nonclassical behavior. Partial measurements performed by alternatively blocking the light impinging on the detectors $D_2$ and $D_3$ were not very reliable as the numbers of detected photons on the two fields separately were too close to the electronic noise of the detection chain. This is an important drawback as, for all calculations that follow based on experimental data, we must take into account the electronic noise that we measured in the absence of light [27].

As the pump fields are pulsed and their duration is longer than the characteristic time of the nonlinear processes, the distributions of the detected photons collected by the pinholes are temporally multimode [25]. The same is also true for the statistical distribution of the sum $m_2+m_3$. Moreover, these distributions should be characterized by the same number of modes [24].

From the experimental point of view, the main difficulty to be overcome was the correct selection of a triplet of coherence areas. In fact, in the CV domain we have to avoid spurious light that could be detrimental to the experimental results; moreover, the interaction scheme presented here involves not only two generated fields, but also a third one, which obviously makes the detection more critical. Finally, we have two pump fields instead of one, and in particular we are not able to exactly measure the effective portions of them that interact into the crystal. In spite of all these difficulties, we characterized the state produced by the interlinked interactions and in particular we proved its quantum nature by performing sub-shot-noise photon-number correlation measurements as a function of the pump fields intensities. In fact, as remarked in Sec. II, the evaluation of the noise reduction

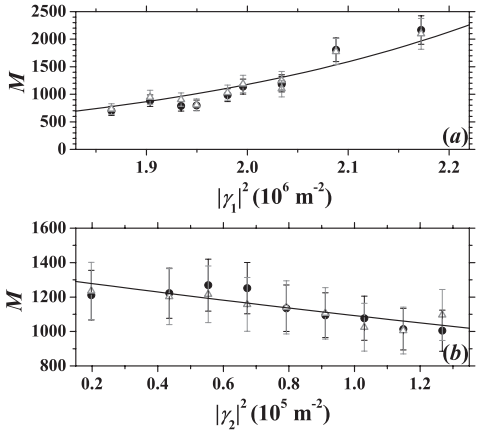


FIG. 3. (a) Evolution of the mean numbers of detected photons as a function of $|\gamma_1|^2$, which is proportional to the intensity of field $a_4$, for $|\gamma_2|^2=8.17\times10^5$ m$^{-2}$. Black circles, measured values of $M_1$; gray triangles, measured values of $M_2+M_3$; solid straight line, fitting curve. (b) Evolution of the mean numbers of detected photons as a function of $|\gamma_2|^2$, which is proportional to the intensity of field $a_5$, for $|\gamma_1|^2=1.52\times10^6$ m$^{-2}$. Black circles, measured values of $M_1$; gray triangles, measured values of $M_2+M_3$; solid straight line, fitting curve.

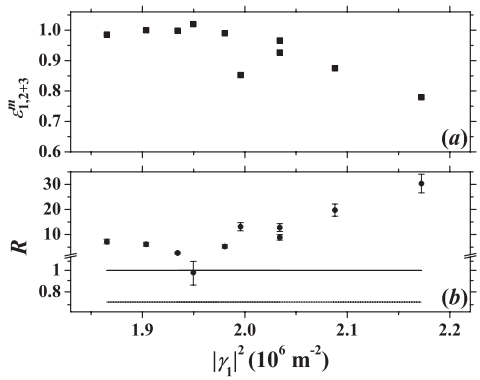


FIG. 4. (a) Intensity correlation coefficient and (b) quantum noise reduction $R$ (note the axis break) as functions of $|\gamma_1|^2$ for $|\gamma_2|^2=8.17\times10^5$ m$^{-2}$.

factor $R$ for the distribution of the difference photocurrent $d=m_1-(m_2+m_3)$ provides a sufficient condition in order to test the quantum nature of the generated state.

We firstly investigated the evolution of the mean number of photons as a function of the intensity of one of the two pumps by keeping fixed the intensity of the other one [29]. In fact, if on one hand this analysis allows us to verify that the mean number of photons does not depend on the correct selection of the coherence areas, on the other one it is essential for the determination of the effective values of the pump fields intensities from the fitting curves.

As a first check we studied the evolution of the mean number of detected photons, $M_1$ and $M_2+M_3$, as a function of the intensity of field $a_4$ for a fixed value of the intensity of field $a_5$. Note that temporal evolution in Eqs. (3) is transformed into spatial evolution by identifying $\sqrt{|g_2|^2-|g_1|^2}t$ with $\sqrt{|\gamma_2|^2-|\gamma_1|^2}z$, $z$ being the effective interaction length [30]. In the experimental condition each $M_j$ represents the total mean number of photons detected beyond each pinhole; actually, it can be expressed as $M_j=\mu\langle m_j\rangle$, where $\mu$ is the number of temporal modes and $\langle m_j\rangle$ the average population of each mode. To vary the intensity of field $a_4$, we changed its energy by means of an adjustable neutral-density filter. For each energy value, measured by means of a movable thermal detector ($D_4$ in Fig. 1, model 03A-P-CAL-SH, Ophir Optronics Ltd., Jerusalem, Israel), we measured the mean number of photons by averaging over 50000 subsequent laser shots. In Fig. 3(a), we show the measured values of $M_1$ and $M_2+M_3$ as functions of $|\gamma_1|^2$, for a fixed value of $|\gamma_2|^2$. Note that $|\gamma_1|^2\propto E_4/(\pi r_4^2\hbar\omega_4\tau_4)$, $E_4$ being the pulse energy of field $a_4$, $\tau_4$ the pulse duration, and $r_4$ the beam radius. The experimental data are displayed together with their common fitting curve, obtained from Eqs. (3) with $|\gamma_2|^2$ as the parameter and $|\gamma_1|^2$ as the variable. In this case we get $|\gamma_2|^2=8.17\times10^5$ m$^{-2}$ and $|\gamma_1|^2$ in the range $1.86\times10^6$–$2.17\times10^6$ m$^{-2}$. Note that, as expected, the experimental data satisfy the photon-number conservation law as they are almost superimposed. The best-fitting curve has been obtained allowing a slight difference in the quantum efficiency values of the detection chains and finding the values from the conservation law. We found $\eta_1=0.31$ and $\eta_{\rm sum}=0.28$. The difference is within the error justified by the tolerance of the pinhole sizes ($\varnothing_1=\varnothing_3=30\pm2$ $\mu$m and $\varnothing_2=50\pm3$ $\mu$m) and it is also justified by possible imperfections in the positioning of the pin-holes at the right distances from the crystal.

As a second check, we studied the evolution of $M_1$ and $M_2+M_3$ as a function of the intensity of field $a_5$, by keeping the intensity of field $a_4$ fixed. To change the energy of field $a_5$ we placed a half-wave plate on the pathway of the infrared pump field. A movable thin-film plate polarizer was used to measure the energy fraction corresponding to the ordinarily polarized component of the field for each step of rotation of the $\lambda/2$ plate. For each energy value, measured by means of the thermal detector ($D_5$ in Fig. 1), we measured the mean number of photons by averaging over 50 000 subsequent laser shots. In Fig. 3(b), we show the measured values of $M_1$ and $M_2+M_3$ as functions of $|\gamma_2|^2$, for a fixed value of $|\gamma_1|^2$. Also, in this case, the experimental data are plotted together with the fitting curve of the two sets of data obtained from Eqs. (3). Obviously, we have to interchange the roles of the pumps: in fact, here $|\gamma_1|^2$ is treated as the parameter and $|\gamma_2|^2$ as the variable. In particular, we obtained $|\gamma_1|^2=1.52\times10^6$ m$^{-2}$ and $|\gamma_2|^2$ in the range $1.97\times10^4$–$1.27\times10^5$ m$^{-2}$. Even in this case, the experimental data satisfy the conservation law as they are almost superimposed and the optimization of the quantum efficiencies still gives very small corrections: $\eta_1=0.283$ and $\eta_{\rm sum}=0.28$.

By exploiting the values of the pump fields intensities obtained from the fitting curves, we can investigate the behavior of the correlation coefficient $\epsilon^m_{1,2+3}$ [see Eq. (10) and of the noise reduction $R$ see Eq. (17)]. First of all, in Fig. 4 we show the intensity correlation coefficient [Fig. 4(a)], and the noise reduction, [Fig. 4(b)] as functions of $|\gamma_1|^2$ by keeping fixed the value of $|\gamma_2|^2$. During these measurements the collection areas were kept fixed (same pinholes located at the same distances as above). The variation of the correlation coefficient as a function of the pump field intensity through

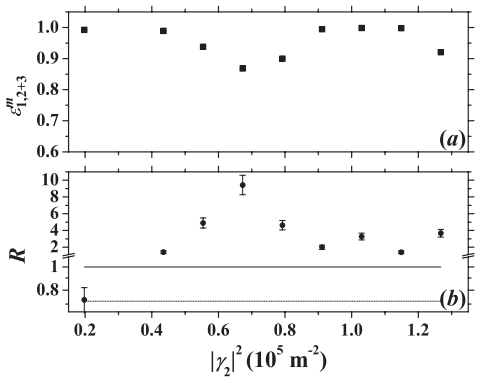


FIG. 5. (a) Intensity correlation coefficient and (b) quantum noise reduction $R$ (note the axis break) as functions of $|\gamma_2|^2$ for $|\gamma_1|^2=1.52\times10^6$ m$^{-2}$.

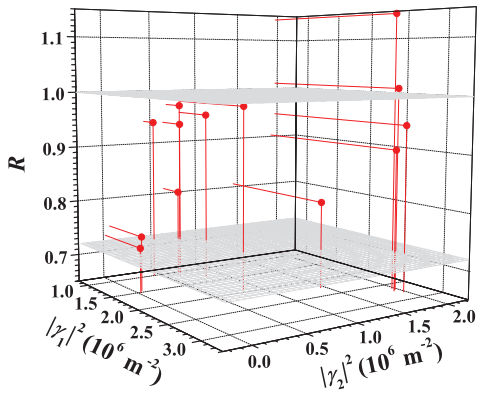


FIG. 6. (Color online) Noise reduction $R$ as a function of $|\gamma_1|^2$ and $|\gamma_2|^2$.

$|\gamma_1|^2$ is indeed not so strong, but the noise reduction factor is critically dependent on the changes in the intensity value. In fact, very much as in the case of the twin-beam state [27], there is an optimum condition at which $R$ is minimum and, correspondingly, the value of the correlation coefficient is maximum. Note that $|\gamma_1|^2$ is larger than $|\gamma_2|^2$ in the entire range of variation. Moreover, we note that increasing the pump intensity and hence $|\gamma_1|^2$ also increases the size of the coherence areas so that they are only partially transmitted by the pinholes. On the other hand, lowering the pump intensity reduces the size of the coherence areas and allows uncorrelated light to pass the pinholes. Note that the values of $R$ corresponding to the selection of more than a single coherence area remain quite close to the shot-noise limit as the information contained in the area is not lost, but only made more noisy. On the contrary, the selection of only a part of the areas causes a loss of information that determines a more remarkable increase of $R$ above the shot-noise limit (note the axis break). This result represents an indication of the need of a perfect matching of the pinhole areas in order to obtain sub-shot-noise correlations.

Second, we investigated the intensity correlation coefficient and the noise reduction as functions of $|\gamma_2|^2$ by keeping fixed the value of $|\gamma_1|^2$. In this case also the collection areas were kept fixed by using the same pinholes as before located at the same distances. The intensity regime in which these measurements were performed is different from the previous one as the absolute values of the two pump-field intensities are smaller than in the other case. However, $|\gamma_2|^2$ is again smaller than $|\gamma_1|^2$ in all its range of variation. For all these reasons, the variations in the experimental values of the correlation coefficient and of the noise reduction are smaller (see Fig. 5). Moreover, the minimum value of $R$ is quite near to the lower limit $R_{\min}=0.72$ fixed by the quantum efficiency. In fact, the use of less intense pumps reduces the quantity of spurious light that can be revealed by the detectors; in addition, the fluctuations of the laser source and the possible discrepancy of its photon-number distribution with respect to the ideal Poissonian statistics play a less important role [31].

As a further investigation, we performed other measurements in order to study how critical is the sub-shot-noise condition with respect to a slight change in the values of the intensities of the two pump fields. In particular, we verified that it is always possible to choose the pumps in such a way that only micrometric adjustments of the pinhole positions are necessary to select the coherence areas. In Fig. 6 we show a number of sub-shot noise measurements obtained for different pairs of pump values. As we can see, not all the measurements reach the optimum minimum value, $R\sim0.72$, due to residual imperfections in the selection of the coherence areas. In particular, as we remarked above, this operation is more critical when the intensity values are higher because other noise sources become important [31]. However, we want to emphasize that there are many possible choices of the pump values that allow us to perform sub-shot-noise measurements thus demonstrating that our scheme is particularly versatile and useful for several applications in different photon-number regimes.

## IV. CONCLUSIONS AND OUTLOOK

In conclusion, we have presented the experimental realization of an entangled state that involves three modes of radiation in the macroscopic regime. We verified the quantum nature of the state produced by our all-optical interaction scheme by means of sub-shot-noise photon-number correlations, which also subsumes the inseparability condition. In particular, we investigated how critical is the sub-shot-noise condition by studying its dependence on the intensities of the two pump fields. In spite of the difficulties in measuring the light of triplet coherence areas correctly and in avoiding the detection of spurious light, we obtained quite relevant results that could be further optimized. In the immediate future we plan to use three acquisition chains instead of only two to separately and simultaneously detect the three fields. Moreover, in order to reduce the noise that is detrimental to the shot-noise reduction factor we still intend to operate in the macroscopic regime, but with lower numbers of photons, and to use hybrid photodetectors, which are endowed with a reasonable quantum efficiency ($\eta\simeq0.4$) and a linear response in the mesoscopic regime (up to a few hundreds of detected photons), instead of the *p-i-n* photodiodes. We also plan to modify our collection system by using optical fibers in order to avoid spurious light and to minimize the uncertainty in the

collection areas. The experimental improvements would make the whole system more easily controllable and suitable for several applications, such as the production of conditional twin-beam states and the generation of quasi-Fock states with a number of photons sensibly greater than one. Overall, our system represents a robust and tunable scheme to obtain nonclassical photon-number correlations in tripartite CV systems thus allowing the simultaneous realization of ghost imaging and ghost diffraction with enhanced sensitivity.

## ACKNOWLEDGMENTS

This work has been supported by MIUR Projects No. PRIN-2005024254-002 and No. FIRB-RBAU014CLC-002.

[1] M. D'Angelo, and Y. Shih, Laser Phys. Lett. **2**, 567 (2005).
[2] A. Gatti, E. Brambilla, and L. A. Lugiato, Prog. Opt. **51**, 251 (2008).
[3] T. Kartaloglu, Z. G. Figen, and O. Aytür, J. Opt. Soc. Am. B **20**, 343 (2003), and references therein.
[4] J. Zhang, C. Xie, and K. Peng, Phys. Rev. A **66**, 032318 (2002).
[5] A. Furusawa, J. L. Sørensen, S. L. Braunstein, C. A. Fuchs, H. J. Kimble, and E. S. Polzik, Science **282**, 706 (1998).
[6] J. Jing, J. Zhang, Y. Yan, F. Zhao, C. Xie, and K. Peng, Phys. Rev. Lett. **90**, 167903 (2003).
[7] T. Aoki, N. Takei, H. Yonezawa, K. Wakui, T. Hiraoka, A. Furusawa, and P. van Loock, Phys. Rev. Lett. **91**, 080404 (2003).
[8] M. Bondani, A. Allevi, E. Puddu, A. Andreoni, A. Ferraro, and M. G. A. Paris, Opt. Lett. **29**, 180 (2004); **29**, 1417(E) (2004).
[9] M. Bondani, A. Allevi, E. Gevinti, A. Agliati, and A. Andreoni, Opt. Express **14**, 9838 (2006).
[10] A. V. Rodionov and A. S. Chirkin, JETP Lett. **79**, 253 (2004).
[11] A. S. Bradley, M. K. Olsen, O. Pfister, and R. C. Pooser, Phys. Rev. A **72**, 053805 (2005).
[12] M. K. Olsen and A. S. Bradley, J. Phys. B **39**, 127 (2006).
[13] O. Pfister, S. Feng, G. Jennings, R. Pooser, and D. Xie, Phys. Rev. A **70**, 020302(R) (2004).
[14] A. S. Villar, M. Martinelli, C. Fabre, and P. Nussenzveig, Phys. Rev. Lett. **97**, 140504 (2006).
[15] E. A. Mishkin and D. F. Walls, Phys. Rev. **185**, 1618 (1969).
[16] M. E. Smithers and E. Y. C. Lu, Phys. Rev. A **10**, 1874 (1974).
[17] A. Ferraro, M. G. A. Paris, M. Bondani, A. Allevi, E. Puddu, and A. Andreoni, J. Opt. Soc. Am. B **21**, 1241 (2004).
[18] A. Ferraro and M. G. A. Paris, Phys. Rev. A **72**, 032312 (2005).
[19] J. Guo, H. Zou, Z. Zhai, J. Zhang, and J. Gao, Phys. Rev. A **71**, 034305 (2005).
[20] N. Piovella, M. Cola, and R. Bonifacio, Phys. Rev. A **67**, 013817 (2003).
[21] M. M. Cola, M. G. A. Paris, and N. Piovella, Phys. Rev. A **70**, 043809 (2004); N. Piovella, M. Cola, and R. Bonifacio, *ibid.* **67**, 013817 (2003).
[22] S. Pirandola, S. Mancini, D. Vitali, and P. Tombesi, Phys. Rev. A **68**, 062317 (2003).
[23] G. X. Li, S. P. Wu, and G. M. Huang, Phys. Rev. A **71**, 063817 (2005).
[24] A. Allevi, M. Bondani, A. Ferraro, and M. G. A. Paris, Laser Phys. **16**, 1451 (2006).
[25] F. Paleari, A. Andreoni, G. Zambra, and M. Bondani, Opt. Express **12**, 2816 (2004).
[26] A. Joobeur, B. E. A. Saleh, T. S. Larchuk, and M. C. Teich, Phys. Rev. A **53**, 4360 (1996).
[27] M. Bondani, A. Allevi, G. Zambra, M. G. A. Paris, and A. Andreoni, Phys. Rev. A **76**, 013833 (2007).
[28] A. Allevi, M. Bondani, M. G. A. Paris, and A. Andreoni, Eur. Phys. J. Spec. Top. **160**, 1 (2008).
[29] A. Allevi, M. Bondani, and A. Andreoni, Proceedings of the Fourth International Workshop ad Memoriam of Carlo Novero, "Advances in Foundations of Quantum Mechanics and Quantum Information with Atoms and Photons," Turin, Italy, 19–23 May 2008, Special Issue of Int. J. Quantum Inf. (in press).
[30] A. Andreoni, M. Bondani, G. M. D'Ariano, and M. G. A. Paris, Eur. Phys. J. D **13**, 415 (2001).
[31] A. Agliati, M. Bondani, A. Andreoni, G. De Cillis, and M. G. A. Paris, J. Opt. B: Quantum Semiclassical Opt. **7**, S652 (2005).